Flow Turbulence Combust (2013) 90:69–94
DOI 10.1007/s10494-012-9424-x

Development of a Low-Reynolds-number k-ω Model for FENE-P Fluids

P. R. Resende · F. T. Pinho · B. A. Younis · K. Kim · R. Sureshkumar

Received: 18 October 2011 / Accepted: 5 November 2012 / Published online: 7 December 2012

Abstract A low-Reynolds-number k-ω model for Newtonian fluids has been developed to predict drag reduction of viscoelastic fluids described by the FENE-P model. The model is an extension to viscoelastic fluids of the model for Newtonian fluids developed by Bredberg et al. (Int J Heat Fluid Flow 23:731–743, 2002). The performance of the model was assessed using results from direct numerical simulations

P. R. Resende · F. T. Pinho (✉)
Centro de Estudos de Fenómenos de Transporte, Departamento de Engenharia Mecânica, Faculdade de Engenharia, Universidade do Porto, Rua Dr. Roberto Frias s/n, 4200-465 Porto, Portugal
e-mail: fpinho@fe.up.pt

P. R. Resende
e-mail: resende@fe.up.pt

B. A. Younis
Department of Civil and Environmental Engineering, University of California, Davis, CA 95616, USA
e-mail: bayounis@ucdavis.edu

K. Kim
Department of Mechanical Engineering, Hanbat National University, 125 Dongseo-daero, Yuseong-gu, Daejeon 305-701, South Korea
e-mail: kkim@hanbat.ac.kr

R. Sureshkumar
Department of Biomedical and Chemical Engineering, Syracuse University, Syracuse, NY 13244, USA
e-mail: rsureshk@syr.edu

Present Address:
P. R. Resende
Engenharia de Controle e Automação, Campus Experimental de Sorocaba, Universidade Estadual Paulista, 18087-180 Sorocaba- SP, Brazil
e-mail: resende@sorocaba.unesp.b

for fully developed turbulent channel flow of FENE-P fluids. It should only be used for drag reductions of up to 50 % (low and intermediate drag reductions), because of the limiting assumption of turbulence isotropy leading to an under-prediction of k, but compares favourably with results from k-ε models in the literature based on turbulence isotropy.

Keywords Drag reduction · Polymer solutions · FENE-P · k-ω turbulence model

1 Introduction

Interest in developing turbulence closures for the prediction of flows with drag-reducing additives has grown over recent years and has fostered a wealth of research on direct numerical simulation (DNS) of turbulent flows with viscoelastic fluids such as polymeric dilute solutions and surfactant solutions. In the DNS investigations with polymer solutions [1–3], the rheology of the fluids has usually been modelled by the Finitely-Extensible-Nonlinear-Elastic constitutive equation with Peterlin's approximation (FENE-P), and, occasionally, by the Oldroyd-B [4] and Giesekus models [5], whereas for the surfactant flow simulations the Giesekus constitutive equation has been more often preferred [6, 7]. In some cases the DNS results were processed to provide Reynolds-averaged data [8, 9] leading to improved understanding of the physical processes involved [10, 11].

First efforts at the development of turbulence closures for drag reduction were reported in the 1970s and invariably involved ad-hoc modifications of mixing length models (see review in Pinho et al. [12]). More physically-based closures were proposed by Malin [13] for purely viscous fluids of variable viscosity, and by Pinho and co-workers [14–17] who adopted a Generalized Newtonian Fluid constitutive equation and mimicked some extensional viscosity effects via a dependence on the third invariant of the rate of deformation tensor. These more physically-based turbulence closures were still not based on a true viscoelastic constitutive equation with memory effects. Therefore, it is only natural that the constitutive models which better describe the rheology of dilute polymer solutions, such as the FENE-P model, are adopted for the development of turbulence closures, even if there are still some discrepancies between the calculated (by DNS) and measured intensities of drag reduction [18].

Previous turbulence closures for FENE-P fluids include the eddy viscosity model of Li et al. [9]. Pinho et al. [12] extended the Newtonian low-Reynolds-number k-ε closure of Nagano and Hishida [19] to viscoelastic fluids and incorporated variable turbulent Prandtl numbers [20] for improved performance. In order to arrive at a closed form turbulence model for FENE-P fluids, Pinho et al. [12] developed closures for new terms appearing in the governing equations such as the nonlinear turbulence distortion term in the evolution equation of the conformation tensor, the so-called NLT_{ij} term [10], the viscoelastic stress work and the viscoelastic-turbulent diffusion appearing in the transport equation of turbulent kinetic energy. These earlier closures were developed on the basis of DNS data, but the models proved suitable only for low drag reduction.

More recently, the same model was significantly improved by Resende et al. [21] who also extended it to the intermediate drag reduction regime. This was achieved by developing a closed form of the exact equation for NLT_{ij} and by introducing

a direct polymer contribution to the eddy viscosity closure. Additionally, in the transport equation for the rate of dissipation of turbulence by the Newtonian solvent, a polymer effect was incorporated. In spite of these improvements the new model still under-predicted the increase of the turbulence kinetic energy (k) with drag reduction.

Recently, Iaccarino et al. [22] developed a k-ε model for FENE-P fluids based on the v^2-f proposals of Durbin [23]. In the v^2-f approach, the eddy viscosity is made to depend on a scalar turbulent velocity scale that brings into the model the more intense wall damping of wall-normal turbulence, obviating the need for the eddy viscosity wall-function, but two extra transport equations for v^2 and f need to be solved. Iaccarino et al. [22] modelled directly the Reynolds-averaged polymer stress without solving the evolution equation for the polymer conformation tensor, thereby reducing the number of coefficients and functions used. The results were generally in good agreement with DNS data both at low and intermediate drag reductions but this model showed some weakness in the prediction of the turbulent kinetic energy. At low drag reduction, the model underpredicted the peak turbulence and matched the turbulence in the log-law region, whereas at intermediate drag reduction the good prediction of peak turbulence comes together with a significant over-prediction of k in the log law region.

Other two-equation turbulence models use the specific rate of turbulence dissipation ($\omega = \varepsilon/k$) instead of the rate of dissipation (ε) itself [24]. Near the walls ω is independent of k, hence k-ω models are numerically more robust there than k-ε models, but in contrast they are overly sensitive to free-stream boundary conditions [25, 26]. An overview of these models can be found in Wilcox [24]. Subsequent improvements of the original k-ω model to obtain the correct asymptotic near-wall behaviour [27, 28] include the exact treatment of viscous cross-diffusion but damping functions had to be introduced. Further developments improved the performance in complex flows with recirculation, as done by Peng et al. [29] and Bredberg et al. [30], who also eliminated the dependence on a wall-function. Bredberg et al. [30] compared their model with the k-ε model of Abe et al. [31], the k-ω model of Wilcox [32], the variant by Lien and Kalitzin [33] of the k-ε-v^2-f model of Durbin, DNS data and experimental data for fully-developed channel flow, backward-facing step flow and rib-roughened channel flow. They found that all turbulence models performed similarly well in fully-developed channel flow, but in recirculating flows their model compared better with DNS and experimental data. In particular, in backward-facing flow the model of Abe et al. [31] under-predicted the recirculation length, whereas both the Wilcox and Durbin's model over-predicted it relative to the DNS and their k-ω model, which was the closest to the DNS data.

The aim of the work reported herein was to develop a k-ω turbulence model for FENE-P fluids valid for both low and intermediate drag reductions. The new model, which incorporates the cross-diffusion term and includes terms associated with fluid elasticity, is calibrated using DNS data for fully-developed channel flow for low and intermediate drag reductions (DR $<$ 30 % and 30 % $<$ DR $<$ 50 %, respectively). It is important at this stage to clarify that the developed k-ω model is an extension to viscoelastic fluids of the Newtonian model of Bredberg et al. [30], presented in Appendix, which has also been slightly changed for improved predictions of Newtonian turbulent channel flow, as explained in Section 2.

The remainder of this paper is organised as follows: the governing equations for the k-ω turbulence model for fluids represented by the FENE-P rheological

constitutive equation are presented in Section 2. Section 3 presents the various closure assumptions proposed. The complete turbulence model is summarized in Section 4, and model assessment against DNS and k-ε model results for fully-developed channel flow is presented in Section 5. The paper closes with the summary of the main conclusions.

2 Governing Equations and Model Development

In the Reynolds-averaged Navier-Stokes framework, the continuity and momentum equations for an incompressible FENE-P fluid take the form [34]:

$$\frac{\partial U_i}{\partial x_i} = 0 \tag{1}$$

$$\rho \frac{\partial U_i}{\partial t} + \rho U_k \frac{\partial U_i}{\partial x_k} = -\frac{\partial \overline{p}}{\partial x_i} + \eta_s \frac{\partial^2 U_i}{\partial x_k \partial x_k} - \frac{\partial}{\partial x_k}\left(\rho \overline{u_i u_k}\right) + \frac{\partial \overline{\tau}_{ik,p}}{\partial x_k}, \tag{2}$$

where η_s is the viscosity coefficient of the Newtonian solvent, $\overline{\tau}_{ik,p}$ is the Reynolds-averaged polymer stress, U_i is the velocity vector, $\overline{p}$ is the mean pressure, ρ is the fluid density and $-\rho\overline{u_i u_k}$ is the Reynolds stress tensor.

An expression for $\overline{\tau}_{ij,p}$ can be obtained by Reynolds-averaging the rheological FENE-P constitutive equation and is given by [35]:

$$\overline{\tau}_{ij,p} = \frac{\eta_p}{\lambda}\left[f\left(C_{kk}\right) C_{ij} - f\left(L\right)\delta_{ij}\right] + \frac{\eta_p}{\lambda}\overline{f\left(C_{kk} + c_{kk}\right) c_{ij}} \tag{3}$$

where λ is the relaxation time of the polymer, η_p is its viscosity coefficient and C_{ij} is the mean conformation tensor. In the FENE-P constitutive equation a dilute polymer solution is modelled as a collection of non-interacting dumbbells, each representing an ultra simplified linear polymer molecule, in a sea of solvent. A dumbbell is represented by two mass-less spheres connected by a nonlinear elastic spring which accounts for the internal entropic force of the molecule. The use of a single dumbbell does not allow the representation of the large number of internal degrees of freedom of the molecule, but nevertheless the modelled molecule can stretch and change orientation. The force balance on each dumbbell relates the viscous drag on the spheres, the Brownian forces due to thermal fluctuations and the internal restoring force on the spring. The constitutive equation results from an averaging process over the configurational space of the local collection of dumbbells due to the force balance on each dumbbell. Then, to arrive at a closed form expression for the polymer stress a closure model is required for the non-linear spring force (the Peterlin approximation of the FENE model [35], where the higher order correlations between the end-to-end vectors are cast in terms of second order correlations). The conformation tensor is simply the average second moment of the end-to-end vector of the dumbbell normalised by its equilibrium length squared so that at rest the conformation tensor relaxes to the unit tensor.

Pinho et al. [12] have shown that the impact of the double correlations (the last term in Eq. 3) to be small at low and intermediate drag reductions and thus $\bar{\tau}_{ij,p}$ will be modelled in this work as:

$$\overline{\tau}_{ij,p} \approx \frac{\eta_p}{\lambda}\left[f\left(C_{kk}\right) C_{ij} - f\left(L\right)\delta_{ij}\right] \tag{4}$$

The functions that appear in this equation have the form [34]:

$$f(C_{kk}) = \frac{L^2 - 3}{L^2 - C_{kk}} \text{ and } f(L) = 1 \tag{5}$$

where L^2 denotes the maximum extensibility of the dumbbell model.

The mean conformation tensor (C_{ij}) which appears in Eq. 3 is determined by Reynolds averaging its instantaneous evolution equation to obtain [35]:

$$\left[\frac{\partial C_{ij}}{\partial t} + U_k \frac{\partial C_{ij}}{\partial x_k} - \underbrace{\left(C_{jk}\frac{\partial U_i}{\partial x_k} + C_{ik}\frac{\partial U_j}{\partial x_k}\right)}_{M_{ij}}\right] + \underbrace{\overline{u_k \frac{\partial c_{ij}}{\partial x_k}}}_{CT_{ij}} - \underbrace{\left(\overline{c_{kj}\frac{\partial u_i}{\partial x_k}} + \overline{c_{ik}\frac{\partial u_j}{\partial x_k}}\right)}_{NLT_{ij}} = -\frac{\overline{\tau}_{ij,p}}{\eta_p} \tag{6}$$

The terms NLT_{ij} and CT_{ij} in Eq. 6 represent viscoelastic cross correlations that are unknown and require closure. The CT_{ij} term is negligible at low and intermediate DR and is therefore neglected. In this study, we adopt the proposal of Resende et al. [21] for NLT_{ij}:

$$\begin{aligned}
NLT_{ij} \equiv{}& \overline{c_{kj}\frac{\partial u_i}{\partial x_k}} + \overline{c_{ik}\frac{\partial u_j}{\partial x_k}} \approx C_{F1}\left(0.055\frac{We_{\tau 0}}{25} + 0.116\right) \\
&\times \frac{C_{ij} \times f(C_{mm})}{\lambda} - C_{F2} We_{\tau 0}^{0.74}\left[C_{kj}\frac{\partial U_i}{\partial x_k} + C_{ik}\frac{\partial U_j}{\partial x_k}\right] + \frac{\lambda}{f(C_{mm})} \\
&\times \left[C_{F3} \times \left(\frac{25}{We_{\tau 0}}\right)^{0.72}\right. \\
&\quad \times \left(\frac{\partial U_j}{\partial x_n}\frac{\partial U_m}{\partial x_k} C_{kn} \frac{\overline{u_i u_m}}{\nu_0\sqrt{2S_{pq}S_{pq}}} + \frac{\partial U_i}{\partial x_n}\frac{\partial U_m}{\partial x_k} C_{kn} \frac{\overline{u_j u_m}}{\nu_0\sqrt{2S_{pq}S_{pq}}} + \frac{\partial U_k}{\partial x_n}\frac{\partial U_m}{\partial x_k}\right. \\
&\qquad \left.\left. \times \left(C_{jn}\frac{\overline{u_i u_m}}{\nu_0\sqrt{2S_{pq}S_{pq}}} + C_{in}\frac{\overline{u_j u_m}}{\nu_0\sqrt{2S_{pq}S_{pq}}}\right)\right)\right] \\
&- \frac{\lambda}{f(C_{mm})} \times f_{F1} \times C_{F4} \times \left(\frac{25}{We_{\tau 0}}\right)^{0.7} \\
&\times \left[C_{jn}\frac{\partial U_k}{\partial x_n}\frac{\partial U_i}{\partial x_k} + C_{in}\frac{\partial U_k}{\partial x_n}\frac{\partial U_j}{\partial x_k} + C_{kn}\frac{\partial U_j}{\partial x_n}\frac{\partial U_i}{\partial x_k} + C_{kn}\frac{\partial U_i}{\partial x_n}\frac{\partial U_j}{\partial x_k}\right] \\
&+ \frac{\lambda}{f(C_{mm})}\left[\frac{C_{\varepsilon_F}}{We_{\tau 0}}\frac{4}{15} \times \frac{C_k \times k \times \omega^N}{(\nu_s + \nu_{\tau_p}) \times \beta} C_{mm} \times f_{F2} \times \delta_{ij}\right]
\end{aligned} \tag{7}$$

where We_{τ_0} is the Weissenberg number, defined as $We_{\tau_0} \equiv \lambda u_\tau^2/\nu_0$, k is the turbulent kinetic energy and S_{ij} is the rate of deformation tensor, $S_{ij} \equiv \left(\partial U_i/\partial x_j + \partial U_j/\partial x_i\right)/2$. The Weissenberg number relies on the friction velocity (u_τ) and ν_0 is the sum of the kinematic viscosities of the solvent and polymer, $\nu_0 = \nu_s + \nu_p$. It is important to realize that even though Eq. 7 looks complex, this closure for NLT_{ij}

is in fact an explicit algebraic equation with a negligible computational cost. It allows the computation of C_{ij} and $\overline{\tau}_{ij,p}$ through Eqs. 4–6, the equations also valid for laminar flow, while maintaining a closure level for NLT_{ij} compatible with the closure level for the Reynolds stress presented below. This is a middle ground modelling option between the use of a full transport equation for NLT_{ij} and the modelling of the polymer stress at a lower level as for the Reynolds stress tensor, but below that used for laminar flow, as done by Iaccarino et al. [22]. In addition, for the specific case of fully-developed turbulent channel flow there is an exact solution of the differential evolution equation for C_{ij} provided in the appendix of Pinho et al. [12], which is used here.

The parameters and damping functions are unchanged from the original reference and are listed in Table 1. The extra C_k coefficient appears due to the definition of ω^N, by adapting the Newtonian dissipation, ε^N, in the k-ω context, $\varepsilon^N = C_k \times k \times \omega^N$.

The Reynolds stress tensor appearing in Eq. 2 is modelled by Boussinesq's linear stress-strain relationship:

$$-\rho\overline{u_i u_j} = 2\rho\nu_T S_{ij} - \frac{2}{3}\rho k\delta_{ij}, \tag{8}$$

where k is the turbulent kinetic energy and ν_T is the eddy viscosity.

In their model for FENE-P fluids, Resende et al. [21] took the eddy viscosity ν_T to be the sum of a Newtonian $\left(\nu_T^N\right)$ and a polymeric $\left(\nu_T^P\right)$ contribution, thus:

$$\nu_T = \nu_T^N - \nu_T^P \tag{9}$$

In this work, we model the Newtonian contribution as a function of the specific rate of dissipation along the lines of the k-ω model [24], thus:

$$\nu_T^N = C_\mu \times f_\mu \times \frac{k}{\omega^N}, \tag{10}$$

The model coefficient and damping function are those of Bredberg et al. [30] except that the original coefficient value of 25 in the damping function f_μ was changed to 28 for improved predictions of velocity in Newtonian turbulent channel flow:

$$\begin{aligned} C_\mu &= 1.0 \text{ and} \\ f_\mu &= 0.09 + \left(0.91 + \frac{1}{R_t^3}\right)\left[1 - \exp\left\{-\left(\frac{R_t}{28}\right)^{2.75}\right\}\right] \text{ with} \\ R_t &= \frac{k}{\omega^N \cdot \nu_S} \end{aligned} \tag{11}$$

Resende et al. [21] modelled the polymeric contribution to the eddy viscosity ν_T^P as a function of the trace of the conformation tensor and introduced a damping function

Table 1 Parameters and damping functions of the NLT_{ij} model

C_{F1}	C_{F2}	C_{F3}	C_{F4}	$C_{\varepsilon F}$	C_k
1.0	0.0105	0.046	1.05	2	0.09
$f_{F1} = \left(1 - 0.8\exp\left(-\frac{y^+}{30}\right)\right)^2$			$f_{F2} = \left(1 - \exp\left(-\frac{y^+}{25}\right)\right)^4$		

depending on the Weissenberg number and distance from the wall $f\left(We_{\tau_0}, y^+\right)$. Their model, which is adopted here unchanged, reads as:

$$\nu_T^P = f\left(We_{\tau_0}, y^+\right) \times \frac{C_{mm}}{\sqrt{L^2}} \times C_\mu \times f_\mu \times \frac{k}{\omega^N}, \tag{12}$$

where $f\left(We_{\tau_0}, y^+\right) = C_\mu^P \times f_\mu^P \times f_{DR}$ with $C_\mu^P = 0.0135 \times \left[\frac{25}{We_{\tau 0}}\right]^{0.12}$,

$$f_\mu^P = \left[1 + 2.55 \times \exp\left(-\frac{y^+}{44}\right)\right] \text{ and } f_{DR} = \left[1 - \exp\left(-\frac{We_{\tau 0}}{6.25}\right)\right]^4. \tag{13}$$

The eddy viscosity model is capable of predicting the correct evolution shown by the DNS data in both low (LDR) and intermediate drag reductions (IDR), namely a decrease in ν_T as DR increases with the Weissenberg number, as shown in Fig. 1. As can also be observed the discrepancies at large y^+ are inherent to the original Newtonian model and not a consequence of viscoelastic modelling. These discrepancies have a negligible impact on both momentum and turbulent kinetic energy predictions in the centreline region because there the eddy viscosity multiplies a vanishingly small rate of deformation. To close the eddy viscosity model, transport equations are solved for k and ω^N, discussed latter. The Reynolds-average polymer stress is provided by the Reynolds-average constitutive equation, discussed next.

The transport equation for k is obtained by taking half the trace of the Reynolds stress transport equation [8]:

$$\rho\frac{Dk}{Dt} + \rho\overline{u_i u_k}\frac{\partial U_i}{\partial x_k} = -\rho\overline{u_k\frac{\partial k}{\partial x_k}} - \frac{\partial\overline{p\prime u_i}}{\partial x_i} + \eta_s\frac{\partial^2 k}{\partial x_k^2} - \eta_s\overline{\frac{\partial u_i}{\partial x_k}\frac{\partial u_i}{\partial x_k}} + \frac{\partial}{\partial x_k}\left(\overline{\tau\prime_{ik}^p u_i}\right) - \left(\overline{\tau\prime_{ik}^p\frac{\partial u_i}{\partial x_k}}\right) \tag{14}$$

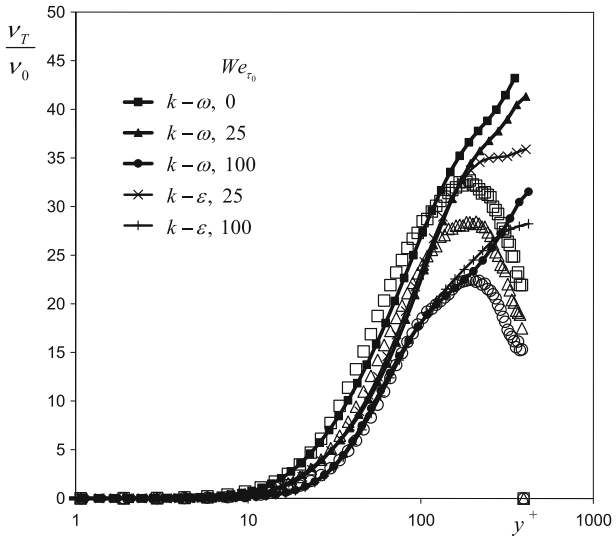

Fig. 1 Comparison between predictions by the k-ω and k-ε [21] models (*lines with close symbols*) of normalized eddy viscosity with DNS data (*open symbols*), for turbulent channel flow at $Re_{\tau 0} = 395$, $L^2 = 900$ and $\beta = 0.9$: □ Newtonian $\left(We_{\tau_0} = 0\right)$, △ $DR = 18$ % $\left(We_{\tau_0} = 25\right)$ and ○ $DR = 37$ % $\left(We_{\tau_0} = 100\right)$

By introducing the definition of instantaneous polymer stress we obtain:

$$\rho\frac{Dk}{Dt} = \underbrace{-\rho\overline{u_i u_k}\frac{\partial U_i}{\partial x_k}}_{\rho P_k} - \underbrace{\left(\overline{\rho u_k \frac{\partial k}{\partial x_k}} + \frac{\partial \overline{p' u_i}}{\partial x_i}\right)}_{\rho Q_k} + \underbrace{\eta_s \frac{\partial^2 k}{\partial x_k^2}}_{\rho D_k^N} - \underbrace{\eta_s \overline{\frac{\partial u_i}{\partial x_k}\frac{\partial u_i}{\partial x_k}}}_{\rho\varepsilon^N}$$
$$+ \underbrace{\frac{\eta_p}{\lambda}\frac{\partial}{\partial x_k}\left[C_{ik}\overline{f\left(C_{mm}+c_{mm}\right)u_i} + \overline{c_{ik} f\left(C_{mm}+c_{mm}\right)u_i}\right]}_{\rho Q^V}$$
$$- \underbrace{\frac{\eta_p}{\lambda}\left[C_{ik}\overline{f\left(C_{mm}+c_{mm}\right)\frac{\partial u_i}{\partial x_k}} + \overline{c_{ik} f\left(C_{mm}+c_{mm}\right)\frac{\partial u_i}{\partial x_k}}\right]}_{\rho\varepsilon^V} \tag{15}$$

where P_k represents the rate of production of k; Q_k the turbulent transport of k by velocity and pressure fluctuations; D_k^N the molecular diffusion of k associated with the Newtonian solvent; ε^N the direct viscous dissipation of k by the Newtonian solvent; Q^V the viscoelastic turbulent transport and ε^V the viscoelastic stress work.

In this work, Q_k and ε^V are modelled along the lines suggested by the previous low-Reynolds-number k-ε models for FENE-P fluids of references [12, 21], namely

$$Q_k = \frac{\partial}{\partial x_i}\left(\frac{\nu_T}{\sigma_k}\frac{\partial k}{\partial x_i}\right) \tag{16}$$

and

$$\varepsilon^V \equiv \frac{1}{\rho}\overline{\tau'_{ik,p}\frac{\partial u_i}{\partial x_k}} \approx 1.37 \times \left[\frac{We_{\tau 0}}{25}\right]^{0.1} \times f_{DR} \times \frac{\eta_p}{\rho\lambda} f\left(C_{mm}\right)\frac{NLT_{mm}}{2}, \tag{17}$$

where the drag reduction function f_{DR} corrects the behaviour for the effect of the Weissenberg number (cf. [21]).

For the viscoelastic turbulent transport (Q^V), the present closure is also based on the proposals of Pinho et al. [12] and Resende et al. [21] with modifications related to the rate of dissipation by the Newtonian solvent (ε^N). In these works ε^N was split into a pseudo-dissipation ($\widetilde{\varepsilon}^N$) and a wall correction (D) according to $\varepsilon^N = D + \widetilde{\varepsilon}^N$. In Pinho et al. [12] D is proportional to the Newtonian solvent viscosity, but here this was found to be inadequate especially at low Weissenberg numbers, leading to predictions of drag increase rather than drag reduction (or to no change in relation to the Newtonian flow). Actually, this deficiency is not as severe as one might think; the Weissenberg number is usually decreased by reducing the relaxation time, but for FENE-P fluids the relaxation time and the polymer viscosity coefficient are related by $\eta_p \to nk_B T\lambda L^2/\left(L^2+5\right)$ in the limit of small Weissenberg numbers, i.e., at small *We* both parameters must be reduced and when this is done simultaneously the model deficiency is reduced. However, the exact equation relating λ and η_p is unknown so there is a real problem at small *We* as *We* is reduced without the concomitant change in *Re*, which Resende et al. [21] solved by making D proportional to the local shear viscosity of the fluid ($\mu = \eta_s + \eta_{\tau_p}$, where $\eta_{\tau_p} = \tau_{xy}^p/\dot{\gamma}$).

By using ω^N instead of ε^N this wall correction D term naturally disappears and the problem of predicting a drag increase at low *We* reappears. The solution of this problem is a modification of the original closures for the viscoelastic turbulent

diffusion of k and ω^N in a way that impacts only the wall region, as was the case with term D in the k-ε model. This modification specifically consists of the direct incorporation of an extra molecular diffusion associated with the local shear polymer viscosity in the transport equations of k and of ω^N, the former being denoted Q_D^V. Consequently, the closure for Q^V becomes now

$$\rho Q^V \equiv \frac{\partial \overline{\tau'_{ik,p} u_i}}{\partial x_k} \approx \underbrace{\frac{\eta_p}{\lambda}\frac{\partial}{\partial x_k}\left[f\left(C_{mm}\right)\left(\frac{C_{ik}FU_i + CU_{iik}}{2}\right)\right]}_{\rho Q_T^V} + \underbrace{\eta_{\tau_P}\frac{\partial^2 k}{\partial x_k^2}}_{\rho Q_D^V}, \tag{18}$$

where Q_T^V is the former Q^V (as in [21]). Q_D^V together with the molecular diffusion by the Newtonian solvent $\left(\eta_s \partial^2 k / \partial x_i \partial x_i\right)$ results in a molecular diffusion by the whole solution, since $\eta_s + \eta_{\tau_p}$ is the local shear viscosity of the FENE-P fluid. Incidentally, the k-ε v^2-f viscoelastic turbulence model of Iaccarino et al. [22] also has a molecular diffusion term proportional to the fluid viscosity, $\eta_s + \eta_{\tau_p}$. The closures for CU_{iik} and $C_{ik}FU_i$ are given by Eqs. 19 and 20, respectively,

$$CU_{iik} = -C_{\beta 1}\sqrt{\frac{25}{We_{\tau 0}}}\frac{\lambda}{f\left(C_{mm}\right)}\left(2\overline{u_i u_m}\frac{\partial C_{ki}}{\partial x_m}\right) - C_{\beta 7}\left(\frac{We_{\tau 0}}{25}\right)^{1.66}\left[\pm 2\sqrt{\overline{u_i^2}}C_{ik}\right] \tag{19}$$

$$C_{ik}FU_i = \frac{C_{FU}}{2}\sqrt{\frac{We_{\tau 0}}{25}}C_{ik}\frac{\partial \overline{u_n u_n}}{\partial x_i} \tag{20}$$

with coefficients $C_{\beta 1} = 0.6$, $C_{\beta 2} = 0.05$ and $C_{FU} = 1$, i.e., they are identical to those used in the context of the k-ε model [21]. It is important to refer that in addition to solving the problem of drag increase at very low We, this closure of Q^V provides an onset of drag reduction at $We_{\tau_0} \approx 5.5$, which is close to the value of $We_{\tau_0} \approx 6.25$ obtained by DNS.

The final form of the transport equation of turbulent kinetic energy is

$$\begin{aligned}\frac{\partial \rho k}{\partial t} + \frac{\partial \rho U_i k}{\partial x_i} = &-\rho\overline{u_i u_k}\frac{\partial U_i}{\partial x_k} + \frac{\partial}{\partial x_i}\left[\left(\eta_s + \rho\nu_{\tau_P} + \rho\frac{\nu_T}{\sigma_k}\right)\frac{\partial k}{\partial x_i}\right] \\ &- \rho C_k \omega k + Q_T^V - \rho\varepsilon^V\end{aligned} \tag{21}$$

and the required values of the turbulent Prandtl number and of the Newtonian coefficient are those of the model of Bredberg et al. [30], i.e. $\sigma_k = 1.0$ and $C_k = 0.09$, respectively.

For a FENE-P fluid, the modelled transport equation for $\tilde{\varepsilon}^N$ takes the form [12]:

$$\begin{aligned}\frac{\partial \rho\tilde{\varepsilon}^N}{\partial t} + \frac{\partial \rho U_i \tilde{\varepsilon}^N}{\partial x_i} = &\underbrace{f_1 C_{\varepsilon_1}\frac{\tilde{\varepsilon}^N}{k}P_k + \eta_s \nu_T\left(1 - f_\mu\right)\left(\frac{\partial^2 U_i}{\partial x_k \partial x_k}\right)^2}_{\rho P_{\varepsilon^N}} \\ &+ \underbrace{\frac{\partial}{\partial x_i}\left[\left(\eta_s\frac{\rho f_t \nu_T}{\sigma_\varepsilon}\right)\frac{\partial \tilde{\varepsilon}^N}{\partial x_i}\right]}_{\rho\left(D_{\varepsilon^N}^N + Q_{\varepsilon^N}\right)} - \underbrace{f_2 C_{\varepsilon_2}\rho\frac{\tilde{\varepsilon}^{N^2}}{k}}_{\rho\Phi_{\varepsilon^N}} + E_{\varepsilon^N}^V\end{aligned} \tag{22}$$

where for compactness we denote P_{ε^N} as the rate of production of ε^N, Q_{ε^N} as the turbulent transport of ε^N by velocity and pressure fluctuations, $D^N_{\varepsilon^N}$ as the molecular diffusion of ε^N by the Newtonian solvent and Φ_{ε^N} as the destruction of ε^N. $E^V_{\varepsilon^N}$ is the viscoelastic term, which is here assumed as a destruction term since the DNS data has shown that ε^N decreases with the viscoelasticity (measured through the Weissenberg number) and drag reduction.

Following Bredberg et al. [30], the derivative of ω^N gives

$$\frac{D\omega^N}{Dt} = \frac{D}{Dt}\left(\frac{\varepsilon^N}{C_k k}\right) = \frac{1}{C_k k}\frac{D\varepsilon^N}{Dt} - \frac{\omega^N}{k}\frac{Dk}{Dt}. \tag{23}$$

By substituting the transport equations of k and ε^N into this expression, and after some lengthy manipulation [36], the final form of the transport equation of ω^N is obtained as:

$$\begin{aligned}\frac{D\omega^N}{Dt} &= \left[\frac{1}{C_k k}P_{\varepsilon^N} - \frac{\omega^N}{k}P_k\right] - \left[\frac{1}{C_k k}\Phi_{\varepsilon^N} - \frac{\omega^N}{k}\varepsilon^N\right] + \left(\frac{\nu_T}{\sigma_{\varepsilon^N}} - \frac{\nu_T}{\sigma_k}\right)\frac{\omega^N}{k}\frac{\partial^2 k}{\partial x_i^2} \\ &+ \frac{\partial}{\partial x_i}\left(\frac{\nu_T}{\sigma_{\varepsilon^N}}\frac{\partial \omega^N}{\partial x_i}\right) + \frac{1}{k}\frac{\partial k}{\partial x_i}\frac{\partial}{\partial x_i}\left[\left(\frac{\nu_T}{\sigma_{\varepsilon^N}} - \frac{\nu_T}{\sigma_k}\right)\omega^N\right] \\ &+ \left[\nu_s\frac{\partial^2\omega^N}{\partial x_i^2}\right] + \underbrace{\frac{1}{k}\left(\frac{\nu_T}{\sigma_{\varepsilon^N}} + \frac{\nu_T}{\sigma_k}\right)\frac{\partial\omega^N}{\partial x_i}\frac{\partial k}{\partial x_i} + \frac{2\nu_s}{k}\frac{\partial\omega^N}{\partial x_i}\frac{\partial k}{\partial x_i}}_{\text{cross diffusion term}} + E^V_{\omega^N}\end{aligned} \tag{24}$$

In the k-ω model of Bredberg et al. [30], the viscous and turbulent cross-diffusion term in Eq. 24 is retained to obtain a better description of the asymptotic near-wall behaviour of k and ω (viz. $k \sim y^2$ and $\omega \sim y^{-1}$) without the need for a specific damping function.

The solvent contribution to Eq. 24 is modelled as in Bredberg et al. [30], and so the modelled transport equation becomes

$$\begin{aligned}\frac{\partial\rho\omega^N}{\partial t} + \frac{\partial\rho U_i\omega^N}{\partial x_i} &= \frac{\partial}{\partial x_i}\left[\left(\eta_s + \rho\nu_{\tau_P} + \rho\frac{\nu_T}{\sigma_\omega}\right)\frac{\partial\omega^N}{\partial x_i}\right] + C_{\omega_1}\frac{\omega^N}{k}P_k - C_{\omega_2}\rho\left(\omega^N\right)^2 \\ &+ \underbrace{\rho\frac{C_\omega}{k}\left(\frac{\eta_s}{\rho} + \nu_{\tau_P} + \nu_T\right)\frac{\partial k}{\partial x_i}\frac{\partial\omega^N}{\partial x_i}}_{\text{cross diffusion term}} + \rho E^V_{\omega^N}.\end{aligned} \tag{25}$$

Term $E^V_{\omega^N}$ introduced earlier in Eq. 24 has a slightly different implementation, i.e., we use Eq. 26 due to the viscoelastic turbulent diffusion contribution to the k equation.

$$E^V_{\omega^N} = \frac{1}{C_k k}E^V_{\varepsilon^N} - \frac{\omega}{k}Q^V_T + \frac{\omega}{k}\varepsilon^V \tag{26}$$

Q^V is given as $Q^V = Q^V_T + Q^V_D$ in Eq. 18 and the closure for Q^V_D (diffusion of k by the local polymer viscosity ν_{τ_P}) was put together with the solvent molecular diffusion and eddy diffusion of k, so it now appears in the cross-diffusion term of the ω^N Eq. 25 as a consequence of Eq. 23. Remember that the incorporation of Q^V_D in the transport equation of k was part of the solution to avoid drag increase at low Weissenberg number flows, but the solution to this problem also involved adding to the transport equation of ω^N a similar molecular diffusion of ω^N by the local polymer viscosity.

Still regarding Eq. 26, the viscoelastic closures for ε^V and Q_T^V are those given by Eqs. 17 and 18, respectively. The $E_{\varepsilon^N}^V$ term is a viscoelastic destruction of ε^N, exactly given by Eq. 27 and requiring a closure.

$$E_{\varepsilon^N}^V = 2\eta_s \frac{\eta_p}{\lambda\left(L^2-3\right)} \overline{\frac{\partial u_i}{\partial x_m}\frac{\partial}{\partial x_k}\left\{\frac{\partial}{\partial x_m}\left[f\left(C_{nn}\right) f\left(\widehat{C}_{pp}\right) c'_{qq} C_{ik}\right]\right\}} \tag{27}$$

In principle, we could use for $E_{\varepsilon^N}^V$ the exact closure developed by Resende et al. [21], written in Eq. 28, but a modification to the numerical values of the coefficients $C_{\varepsilon_{F1}}$ and $C_{\varepsilon_{F2}}$ was required to correct and improve the predictions of the Newtonian dissipation quantity, ε^N (so that the k-ω model predicts ε^N as well as the k-ε model). More details on the development of the closure of $E_{\varepsilon^N}^V$ can be found in [21].

$$E_{\varepsilon^N}^V \approx -f_5 \times f_{DR} \times \frac{(1-\beta)}{We_{\tau 0}} \frac{\varepsilon^{N^2}}{k} \times \left[C_{\varepsilon F1}\left(\frac{We_{\tau 0}}{25}\right)^{0.72} \frac{\varepsilon^V}{\varepsilon^N} + C_{\varepsilon F2}\left(\frac{25}{We_{\tau 0}}\right)^{1.56} \frac{\left(C_{mm} \times f\left(C_{mm}\right)\right)^2}{\left(L^2-3\right)}\right] \tag{28}$$

The two viscolastic damping functions of $E_{\varepsilon^N}^V$ remain unchanged as $f_5 = [1 - \exp(-y^+/50)]$ and f_{DR}, but the coefficients are $C_{\varepsilon F1} = 400$ and $C_{\varepsilon F2} = 1$.

The capacity of the closure for $E_{\varepsilon^N}^V$ to predict well in both the k-ε and k-ω turbulence models, with minor adjustments to the numerical values of coefficients, suggests the fairness of the assumptions invoked to develop the closure for $E_{\varepsilon^N}^V$ by Resende et al. [21].

The remaining coefficients are those used for the Newtonian model, $C_\omega = 1.0$, $C_{\omega_1} = 0.49$, $C_{\omega_2} = 0.072$ and $\sigma_\omega = 1.8$, with a correction in the coefficient C_ω for which we use 1.0 rather than 1.1. Note that this change in C_ω is in line with the correction of the coefficient in the damping function f_μ from a numerical value of 25 to a value of 28, which was aimed at improving the Newtonian predictions for channel flow.

To summarize, this low-Reynolds number k-ω model is an extension of Bredberg et al.'s [30] model to account for viscoelastic FENE-P fluids. Only the eddy viscosity and NLT_{ij} closures are mathematically transformed from the corresponding closures developed in the context of the k-ε model of Resende et al. [21], whereas the closures for the cross-diffusion term, the destruction of ω^N and the viscoelastic turbulent diffusion contain specific developments.

3 Results and Discussion

The turbulence model was tested against DNS data for FENE-P fluids in a viscoelastic turbulent channel flow. The simulations were performed at $DR = 18$ % and 37 % ($We_{\tau 0} = 25$ and $We_{\tau 0} = 100$, respectively, with $We_{\tau_0} \equiv \lambda u_\tau^2/\nu_0$) and with Reynolds number $Re_{\tau 0} = 395$ ($Re_{\tau_0} = u_\tau h/\nu_0$ based on the friction velocity (u_τ), the channel half-height (h) and the zero shear-rate kinematic viscosity of the solution, which is the sum of the kinematic viscosities of the solvent and polymer $\nu_0 = \nu_s + \nu_p$), maximum extension of the conformation tensor $L^2 = 900$ and the viscosity ratio $\beta = 0.9$ ($\beta \equiv \nu_s/\nu_0$).

Throughout this paper the definition of drag reduction used is that introduced by the literature on DNS of viscoelastic fluids [37], namely the ratio of the wall shear stress reduction in viscoelastic flow relative to the wall shear stress for the Newtonian flow at the same mass flow rate, as in Eq. 29.

$$DR = 1 - \frac{\tau_{w,\text{Viscoelastic}}}{\tau_{w,\text{Newtonian}}} = 1 - \left(\frac{u_{\tau,\text{Viscoelastic}}}{u_{\tau,\text{Newtonian}}}\right)^2 \tag{29}$$

Using this definition the DR intensity reported as DR is that of the DNS data, whereas the DR obtained using exclusively the simulations by the turbulence models is denoted DR*. To compute DR for the DNS data, and according to the literature [37], the friction velocity for the drag-reduced flow, $u_{\tau,\text{Viscoelastic}}$, is obtained from the definition of the Reynolds number Re_{τ_0} and the friction velocity for the corresponding Newtonian flow (meaning at the same flow rate of the viscoelastic flow) can be calculated (or approximated) using Dean's correlation,

$$u_{\tau,\text{Newtonian}} = \left(\frac{0.073}{2} Re_m^{-1/4} U_m^2\right)^{1/2} \tag{30}$$

where the mean flow Reynolds number $Re_m = 2hU_m/\nu_w$ is based on the bulk mean velocity U_m and the solution viscosity at the wall (ν_w). To compute DR* the friction velocity for the viscoelastic fluid is obtained also from the Reynolds number, whereas the friction velocity for the corresponding Newtonian flow is that given by the specific turbulence model at the same mass flow rate as the viscoelastic flow.

The governing equations were solved using a finite-volume code specifically developed for boundary layer flows. The original code is described in Younis [38] and was modified for FENE-P fluids. The finite-volume code uses staggered meshes to ensure pressure-velocity-polymer stress coupling in the solution of the governing equations for one- or two-dimensional turbulent boundary layers. In the present implementation for fully-developed channel flow and in order to deal with the FENE-P fluid model, the viscoelastic stress divergence term was added to the momentum equation, volume-integrated and the corresponding stress flux discretized by central differences and added to the source term. The evolution equation of the conformation tensor in fully-developed channel flow was analytically solved by Pinho et al. [12] (cf. its Appendix A) and provides the ensuing algebraic equations for the conformation tensor provided the closure for NLT_{ij} is known. For the transport equations of k and ω the additional terms associated with the FENE-P model were incorporated and discretized also with central differences. No-slip boundary conditions were applied at the wall with $U = k = 0$. The specific rate of dissipation ω follows a well defined asymptotic behaviour described by Wilcox [24]. Since the FENE-P polymer solution has a viscosity given by the sum of the solvent and polymer viscosities, Wilcox's asymptotic expression for Newtonian fluids was modified to incorporate the local total shear viscosity by the inclusion of the corresponding kinematic polymeric contribution (ν_{τ_P}):

$$\omega^N \to \frac{2\left(\nu_S + \nu_{\tau_P}\right)}{C_k \cdot y^2} \tag{31}$$

Grid-independent solutions were obtained using a computational mesh with 99 cells non-uniformly distributed across the channel width. The expansion factor of the

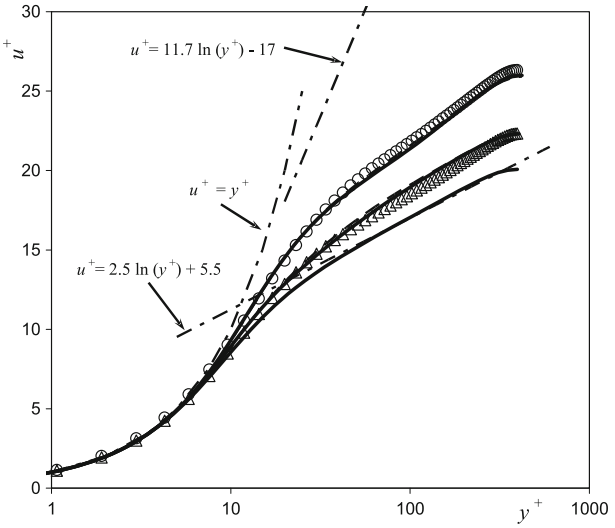

Fig. 2 Comparison between predictions of the mean velocity by this model (*solid lines*), Resende et al.'s model [21] (*dashed lines*) and DNS data (*symbols*), for turbulent channel flow at $Re_{\tau 0} = 395$, $L^2 = 900$ and $\beta = 0.9$: $\triangle$ $DR = 18\ \%$ $\left(We_{\tau_0} = 25\right)$ and $\bigcirc$ $DR = 37\ \%$ $\left(We_{\tau_0} = 100\right)$

mesh was 1.13 (ratio of widths of consecutive control volumes), the smallest cell size near the wall had a dimensionless width $\Delta y/H = 0.00033$, where H is the channel half-width, so that each viscous sublayer was resolved by around 10 computational cells.

In Fig. 2 the predicted mean velocity profiles are compared with DNS data for $DR = 18\ \%$ and $37\ \%$ and with the predictions of Resende et al. [21] obtained with a k-ε model. The k-ω predictions coincide with those of the previous k-ε model and show good agreement with the DNS data. The monotonic shift of the log-law region with DR is well captured, as is the correct evolution in the buffer-layer. We also compare in Table 2 the values of DR^* for the predictions by the k-ω and k-ε models with the values of DR pertaining to the DNS simulations. Although the velocity profiles in Fig. 2 coincide for both turbulence models, the values of DR^* are slightly over-predicted, especially for the k-ε model at $We_{\tau_0} = 25$, because of the different Newtonian predictions of the base Newtonian turbulence models. This further emphasizes the relevance of choosing a Newtonian turbulence model with a good performance as a basis for the development of the viscoelastic closures and suggests that the k-ω model of Bredberg et al. [30] used here is a better candidate than the model of Nagano and Hishida [19] used by Resende et al. [21].

The impact of the Weissenberg number variation on the prediction of the velocity profile and the limits of the model can be observed in Fig. 3, where the k-ω turbulence model is able to reach $DR \approx 47\ \%$, corresponding to a maximum Weissenberg

Table 2 Comparison between the drag reductions predicted by the viscoelastic turbulence models and the DNS simulation for $L^2 = 900$, $Re_{\tau_0} = 395$ and $\beta = 0.9$

	DR^* (%)		DR (%)
	k-ω model	k-ε model [21]	DNS
$We_{\tau_0} = 25$	18	19.6	18
$We_{\tau_0} = 100$	39	39	37

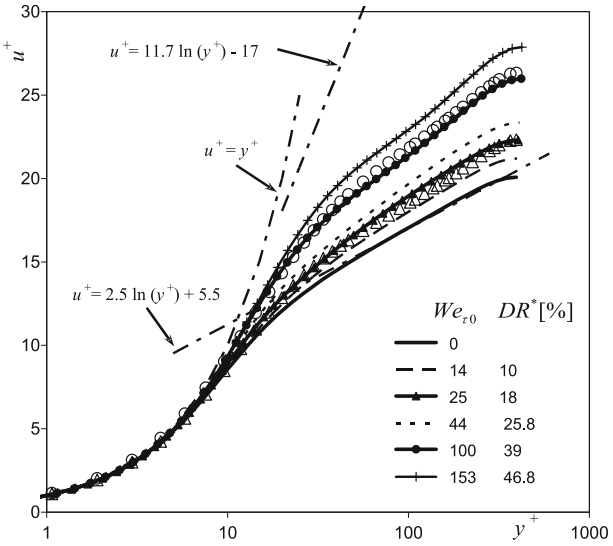

Fig. 3 Comparison between predictions of the mean velocity (*lines with symbols*) with DNS data (*open symbols*: $\triangle$ $DR = 18$ % $\left(We_{\tau_0} = 25\right)$ and $\bigcirc$ $DR = 37$ % $\left(We_{\tau_0} = 100\right)$) for turbulent channel flow at $Re_{\tau 0} = 395$, $L^2 = 900$, $\beta = 0.9$ and different Weissenberg numbers

number $We_{\tau_0} = 153$, with a maximum deviation of 10 % relative to the correlation of Li et al. [9] presented below. This is well within the intermediate range of DR. Above these values the predictions by both models show large discrepancies relative to the DNS data, with an over-prediction of the drag reduction intensity and an under-prediction of k, as discussed next.

Li et al. [9] used extensive DNS data sets to develop a correlation for the drag reduction intensity DR as a function of We_{τ_0}, Re_{τ_0} and the maximum molecular extensibility of the dumbbell (L). The correlation is of the form:

$$DR = 80\left[1 - \exp\left(-0.0275L\right)\right] \times \left\{1 - \exp\left[-0.025\left(We_{\tau_0} - We_{\tau_0,c}\right)\left(\frac{Re_{\tau_0}}{Re_{\tau_0,r}}\right)^{-0.225}\right]\right\} \tag{32}$$

where $We_{\tau_0,c} = 6.25$ and $Re_{\tau_0,r} = 125$.

In Table 3 the drag reduction predicted by the k-ω model is compared with that of Eq. 32 and with the DNS data for several values of the Weissenberg number. While there is a fairly good agreement for large We_{τ_0}, at low We_{τ_0} (such as at $We_{\tau_0} = 25$) there is a large difference in DR* relative to the correlation but this is largely due to the under-prediction of the drag reduction by Li et al.'s [9] expression at LDR, as explained in [9].

Table 3 Comparison between the drag reduction predicted by the turbulence models (DR*), the DNS simulation (DR) with Li et al.'s [9] equation for $L^2 = 900$, $Re_{\tau_0} = 395$ and $\beta = 0.9$

We_{τ_0}	14	25	44	100	153
Present model (DR*)	10	18	25.8	39	46.8
k-ε model [21] (DR*)	9	19.6	27.6	39	43.7
Li et al. [9] equation (DR)	6.2	13.6	23.3	37.6	43
DNS data	–	18	–	37	–

For $L^2 = 900$ the k-ε model of Resende et al. [21] behaves similarly to the present model as shown in Tables 2 and 3, but upon increasing L^2 and We_{τ_0} the $k-\varepsilon$ model predictions deviate significantly from the equation of Li et al. [9]. The predictions of the present k-ω model also deviate from Li's equation, but to a much smaller extent. For instance, with $L^2 = 3600$, $Re_{\tau_0} = 270$, $\beta = 0.9$ and $We_{\tau_0} = 30$, the present k-ω model predicted $DR^* = 23$ % against $DR = 25.4$ % by Li et al.'s [9] equation, whereas the k-ε model predicted $DR^* = 17$ %. In order to assess the effect of the Reynolds number on the model predictions, a set of simulations was undertaken with the present model at $Re_{\tau_0} = 500$ with $L^2 = 900$. For $We_{\tau_0} = 25$ DR^* increased from 18 % at $Re_{\tau_0} = 395$ to 20 % at $Re_{\tau_0} = 500$ while for $We_{\tau_0} = 100$ the corresponding increase in DR^* was from 39 % to 43 %. The equation of Li et al. [9], which has been developed on the basis of DNS data for $125 < Re_{\tau_0} < 395$, predicts values of DR at $Re_{\tau_0} = 500$ similar to those predicted at $Re_{\tau_0} = 395$.

The turbulent kinetic energy predictions are plotted in Fig. 4. The predicted peak values decrease with DR, in contrast with the DNS data, and this represents a deficiency of the model. The model of Resende et al. [21] shows the same deficiency. The evolution of the predictions of k with We_{τ_0} is shown in Fig. 5 where we observe a continuous decrease in k, a defect of the present model also present in the k-ε model of Resende et al. [21]. This deficiency limits the application of the present model up to drag reduction rates of about 50 %.

The reduction of k is related to the inherent incompatibility between the eddy viscosity closure used and the physics of the drag reducing fluids. Experiments and DNS on drag reduction flows show that with increased Weissenberg number, the Reynolds shear stress decreases, but the turbulent kinetic energy increases. Since the eddy viscosity closure models the Reynolds shear stress in proportion to k^2, a reduction in the Reynolds shear stress requires a reduction in this turbulent velocity scale, when it actually increases. In an attempt to resolve this problem Pinho et al. [12] incorporated the viscoelastic stress work in the turbulence length scale,

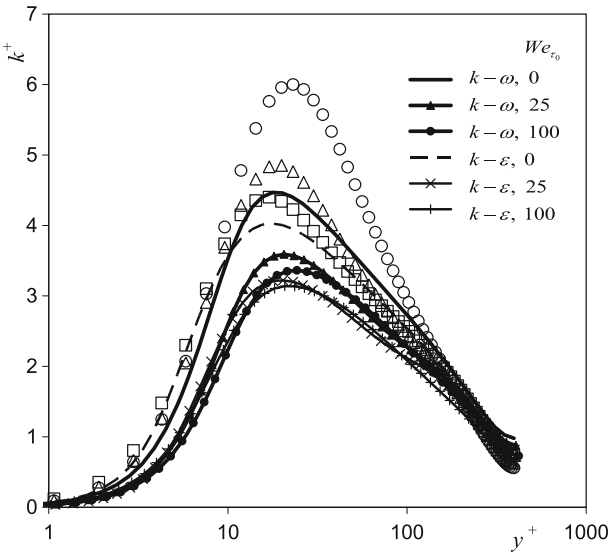

Fig. 4 Comparison between predictions of the turbulent kinetic energy by this model (*lines with symbols*), by the k-ε model of Resende et al. [21] and DNS data (*open symbols*), for turbulent channel flow at $Re_{\tau 0} = 395$, $L^2 = 900$ and $\beta = 0.9$: □ Newtonian $\left(We_{\tau_0} = 0\right)$, △ $DR = 18$ % $\left(We_{\tau_0} = 25\right)$ and ○ $DR =$ 37 % $\left(We_{\tau_0} = 100\right)$

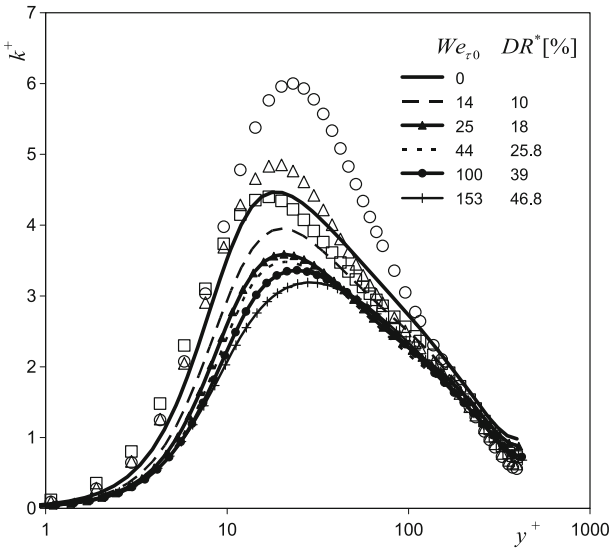

Fig. 5 Comparison between the predictions of the turbulent kinetic energy (*lines with symbols*) with DNS data (*open symbols*): □ Newtonian $(We_{\tau_0} = 0)$, △ $DR = 18$ % $(We_{\tau_0} = 25)$ and ○ $DR =$ 37 % $(We_{\tau_0} = 100)$ and effect of Weissenberg number for turbulent channel flow at $Re_{\tau 0} = 395$, $L^2 = 900$ and $\beta = 0.9$

whereas Resende et al. [21] and the present model consider instead a polymeric contribution to the eddy viscosity subtracting the standard Newtonian eddy viscosity, but both approaches were not effective enough to solve this issue. Incidentally, a fairly successful alternative is that of Durbin [23], also implemented by Iaccarino et al. [22] for FENE-P fluids, who relate the turbulent velocity scale to the transverse normal Reynolds stress. However, this approach is more expensive since it requires the additional numerical solution of two differential equations, and introduces other difficulties in geometries with more than one wall. The solution of this problem is certainly a major motivation for future work with this type of models.

The profiles of the predicted dissipation rate are presented in Fig. 6, normalized by the friction velocity and the zero shear rate kinematic viscosity, including the DNS data and the predictions of [21]. In the buffer and log layers the predictions by both the k-ω model and k-ε model of [21] are similar and agree with the DNS data. Elsewhere there are significant differences, which are also present for Newtonian fluids. These differences require a correction in the coefficient values of the $E^V_{\varepsilon^N}$ closure, which has a direct impact on the predictions of ε^N. The behaviour of the rate of dissipation of k with We_{τ_0} is well captured by the model in the log law, and the buffer layers, as shown in Fig. 7, but very close to the wall there exist differences between the predictions and the DNS, a consequence of the k-ω Newtonian model. The saturation of ε^{N+} observed to occur at large We_{τ_0} is also well captured: we see that at large Weissenberg numbers ($We_{\tau_0} = 100$ and 153) the profiles of ε^{N+} are essentially the same.

Figure 8a–e compare the predictions of NLT^*_{ij} for both the k-ω and k-ε models for $DR = 18$ % and 37 %. NLT^*_{ij} is defined as $NLT_{ij}h/u_\tau$. For each component the predictions by the two models are similar, with the former model showing better predictions than the latter for NLT^*_{11} and the trace NLT^*_{kk} and the other way for the other components. The main features of these predictions are the increase of the peak value of NLT^*_{ij} with DR and its shift away from the wall, which becomes more intense in the log-law region. For all normal components of NLT_{ij} there is an

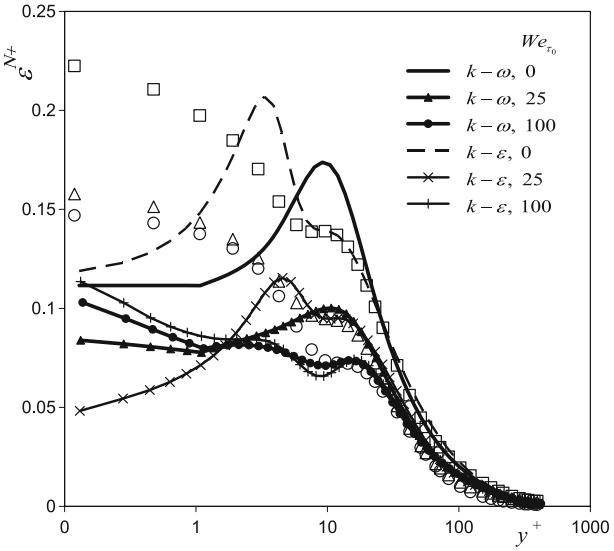

Fig. 6 Comparison between predictions of the Newtonian kinetic energy dissipation by this model (*lines with symbols*), by the *k*-ε model of Resende et al. [21] and DNS data (*open symbols*), for turbulent channel flow at $Re_{\tau 0} = 395$, $L^2 = 900$ and $\beta = 0.9$: □ Newtonian $\left(We_{\tau_0} = 0\right)$, △ $DR = 18$ % $\left(We_{\tau_0} = 25\right)$ and ○ $DR =$ 37 % $\left(We_{\tau_0} = 100\right)$

underprediction of the peak value for $DR = 37$ %, whereas for the shear component there is an overprediction.

NLT^*_{22} (or NLT^*_{yy}) and its variation with We_{τ_0} is shown in Fig. 9a. For compactness this component of the NLT^*_{ij} tensor is the only one presented there because of the high impact in the calculation of the conformation tensor, except on C_{33} component (the behaviour of the predictions with We_{τ_0} variation are similar in the other components). There is a rapid increase at values of DR less than 30 %, after which the maximum value of NLT^*_{22} decreases slowly to stabilize at intermediate DR, as at DR = 37 %. The behaviour of the invariant NLT^*_{kk} is plotted in Fig. 9b and shows also a rapid increase with We_{τ_0} at the low DR regime, followed by a slow increase and saturation at intermediate DR. Since the streamwise normal component is the

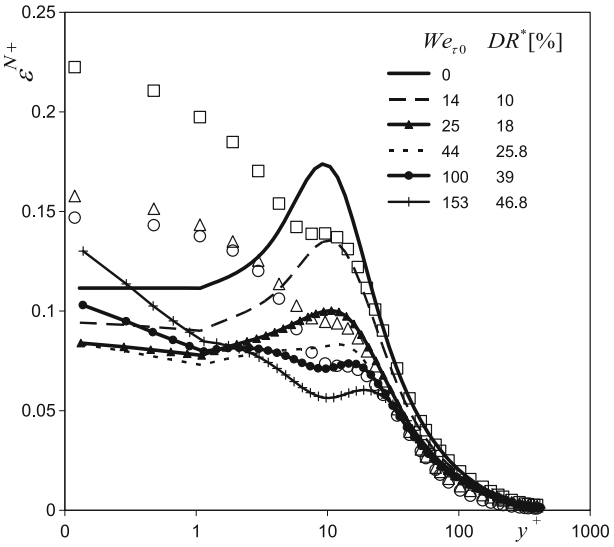

Fig. 7 Comparison between the predictions of the solvent kinetic energy dissipation (*lines with symbols*) with DNS data (*open symbols*): □ Newtonian $\left(We_{\tau_0} = 0\right)$, △ $DR = 18$ % $\left(We_{\tau_0} = 25\right)$ and ○ $DR = 37$ % $\left(We_{\tau_0} = 100\right)$ and effect of Weissenberg number for turbulent channel flow at $Re_{\tau 0} = 395$, $L^2 = 900$ and $\beta = 0.9$

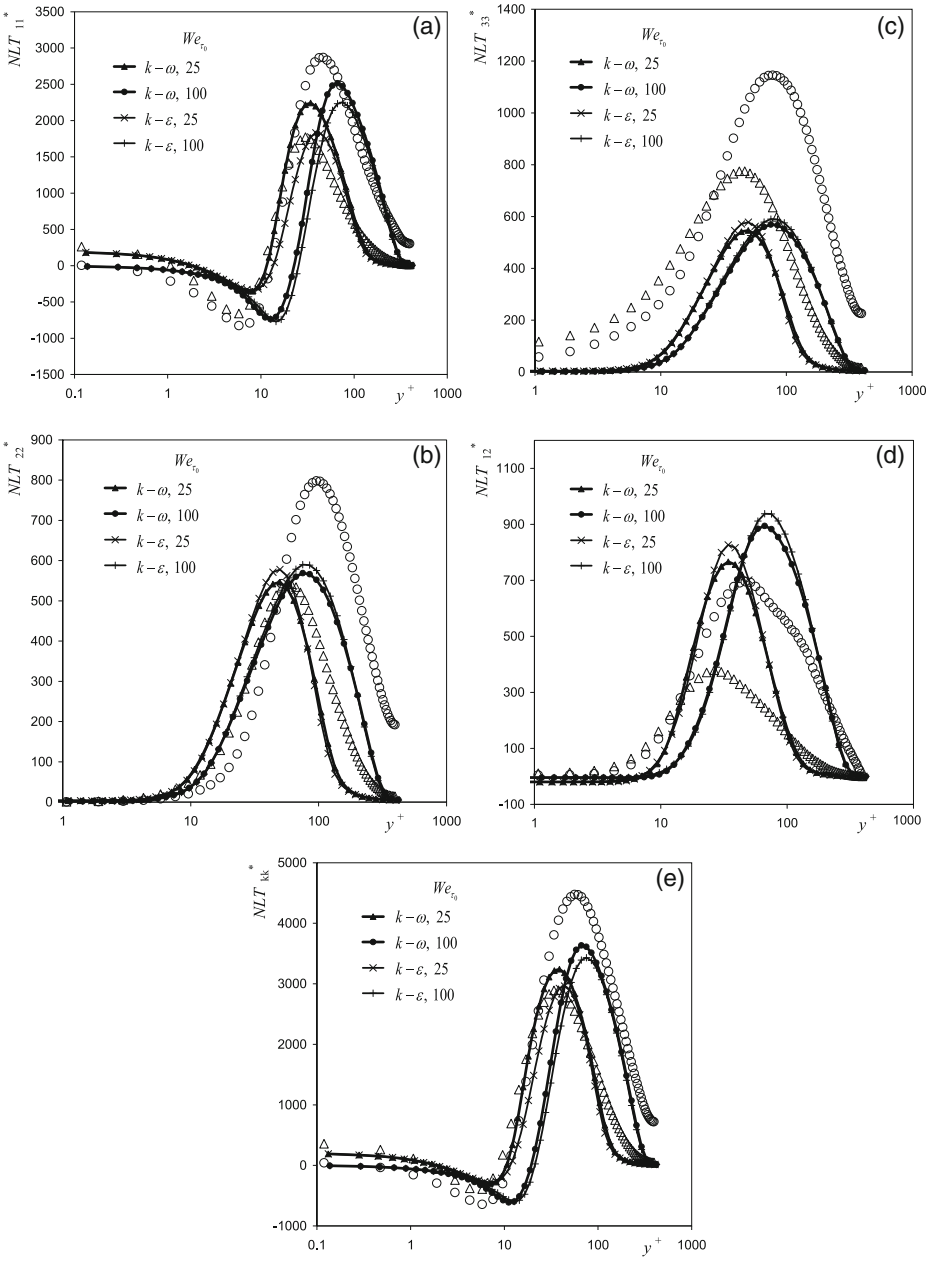

Fig. 8 Comparison between predictions of NLT^*_{ij} by this model (*lines with symbols*), by the k-ε model of Resende et al. [21] and DNS data ($\triangle$ $DR = 18$ % $\left(We_{\tau_0} = 25\right)$ and $\bigcirc$ $DR = 37$ % $\left(We_{\tau_0} = 100\right)$), for turbulent channel flow at $Re_{\tau 0} = 395$, $L^2 = 900$ and $\beta = 0.9$: **a** NLT^*_{11}; **b** NLT^*_{22}; **c** NLT^*_{33}; **d** NLT^*_{12}; **e** NLT^*_{kk}

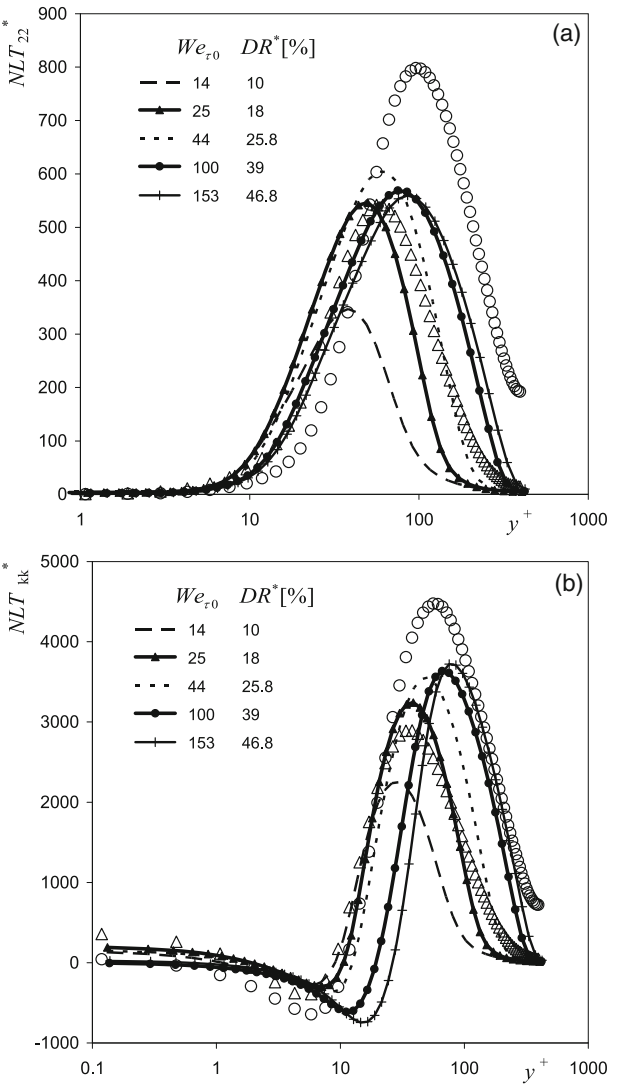

Fig. 9 Comparison between the predictions of NLT^*_{ij} (*lines with symbols*) with DNS data (*open symbols*: $\triangle$ $DR = 18$ % $\left(We_{\tau_0} = 25\right)$ and $\bigcirc$ $DR = 37$ % $\left(We_{\tau_0} = 100\right)$) and effect of Weissenberg number for turbulent channel flow at $Re_{\tau 0} = 395$, $L^2 = 900$ and $\beta = 0.9$: **a** NLT^*_{22} and **b** NLT^*_{kk}

main contribution to NLT^*_{kk}, NLT^*_{11} has a similar behaviour, but is not shown here for compactness.

The predictions of the viscoelastic stress work in Fig. 10 show higher values for the k-ω model than for the k-ε. Specifically, there is a slight overprediction of ε^V for $DR = 37$ %, whereas at low DR both turbulence models under-predict the DNS data. The variation of the viscoelastic stress work with We_{τ_0} is shown in Fig. 11 and exhibits a rapid increase in ε^{V+} at low drag reduction, reaching a maximum at $We_{\tau_0} = 25$, (corresponding to $DR = 18$ %), followed by a decrease with the peak value moving away from the wall, whereas the DNS data shows ε^{V+} always increases with We_{τ_0}. It is also possible to visualize a saturation effect, the reduction of the peak value variation as we increase DR above 37 %, which shows an asymptotic variation towards the maximum drag reduction.

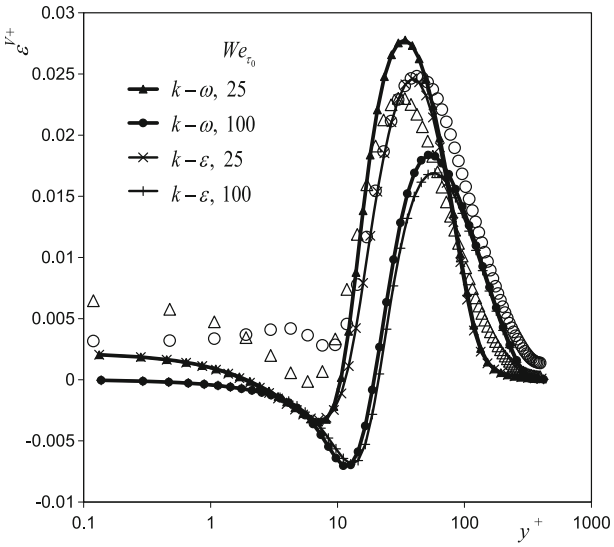

Fig. 10 Comparison between predictions of the viscoelastic dissipation by this model (*lines with symbols*), by the *k*-ε model of Resende et al. [21] and DNS data (*open symbols*), for turbulent channel flow at $Re_{\tau 0} = 395$, $L^2 = 900$ and $\beta = 0.9$: $\triangle$ $DR = 18$ % $\left(We_{\tau_0} = 25\right)$ and $\bigcirc$ $DR = 37$ % $\left(We_{\tau_0} = 100\right)$

The predictions of NLT^*_{ij} and of ε^V are all related and as general comment on these sets of data we can say that in spite of a general improvement over the predictions of *k*-ε model of Resende et al. [21] at the intermediate DR regime (i.e., for $DR \approx 37$ %), these were not enough to eliminate the main deficiency, the under-prediction of *k*, as in the the *k*-ε model. This is ultimately rooted on the turbulence isotropy concept. In all our attempts to improve the prediction of *k* using both models, the prediction of the other quantities have deteriorated. Certainly we could match the predicted *k* with DNS but only at the cost of an over-prediction of ε^N. Since the closures for NLT_{ij} and ε^V also depend on a deficient prediction of *k*, the adoption of a model

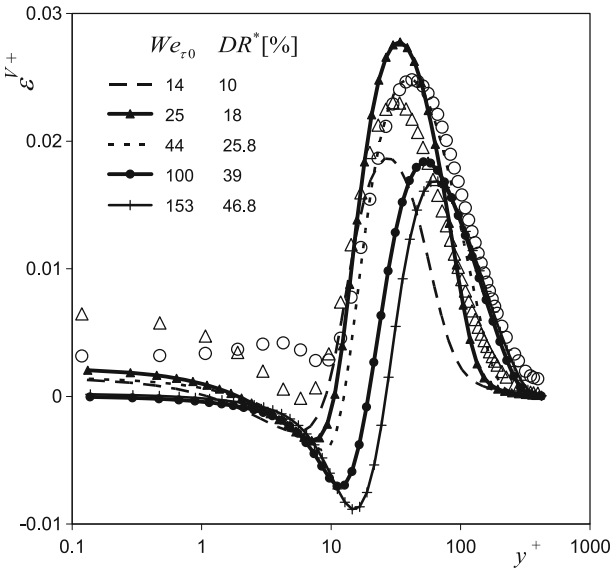

Fig. 11 Comparison between the predictions of the viscoelastic dissipation (*lines with symbols*) with DNS data (*open symbols*: $\triangle$ $DR = 18$ % $\left(We_{\tau_0} = 25\right)$ and $\bigcirc$ $DR = 37$ % $\left(We_{\tau_0} = 100\right)$) and effect of Weissenberg number for turbulent channel flow at $Re_{\tau 0} = 395$, $L^2 = 900$ and $\beta = 0.9$

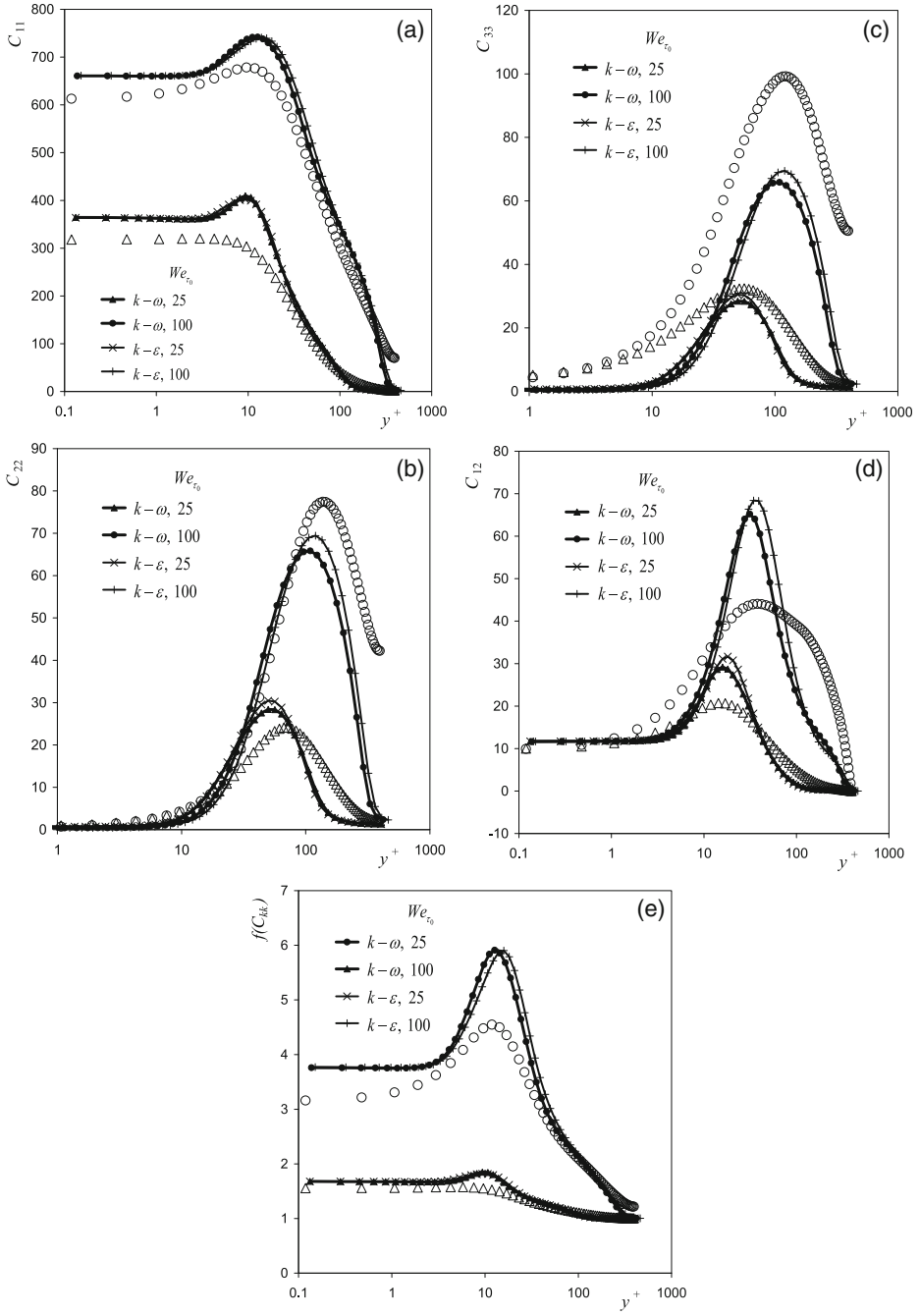

Fig. 12 Comparison between the predictions of the conformation tensor (*lines with symbols*) with DNS data (*open symbols*: $\triangle$ $DR = 18$ % $\left(We_{\tau_0} = 25\right)$ and $\bigcirc$ $DR = 37$ % $\left(We_{\tau_0} = 100\right)$) for turbulent channel flow at $Re_{\tau 0} = 395$, $L^2 = 900$, $\beta = 0.9$ and different Weissenberg numbers: **a** C_{11}; **b** C_{22}; **c** C_{33}; **d** C_{12} and **e** $f(C_{kk})$

not based on turbulence isotropy will allow the correct prediction of k, ε^N and, by recalibration, of NLT_{ij} and ε^V.

The predictions of the NLT_{ij} tensor have a direct impact on the prediction of the conformation tensor, according to Eq. 6, as can be observed by comparing the predictions of NLT^*_{ij} in Fig. 8 and those of the conformation tensor in Fig. 12a–d. The predictions of all components of C_{ij} are fair except for C_{33}, where a large deficit relative to the DNS data is seen as a consequence of a deficit in the prediction of

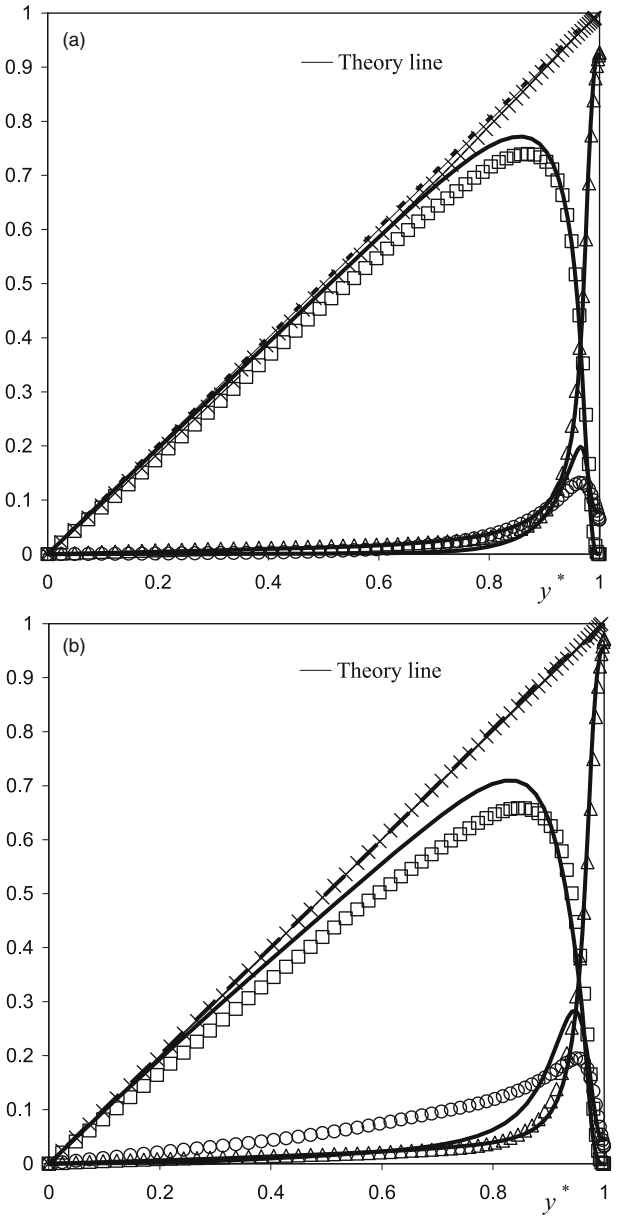

Fig. 13 Comparison between the predictions (*lines*) and DNS data (*open symbols*) for normalized shear stresses (τ_N^+, τ_p^+, $-\overline{u_1u_2}^+$) in turbulent channel flow with $Re_{\tau 0} = 395$, $L^2 = 900$ and $\beta = 0.9$. ($\triangle$ and *line*) τ_N^+, ($\bigcirc$ and *line*) τ_p^+, ($\square$ and *line*) $-\overline{u_1u_2}^+$; ($\times$ and *dashed line*) sum of stresses: **a** $DR = 18\ \%\ \left(We_{\tau_0} = 25\right)$; **b** $DR = 37\ \%\ \left(We_{\tau_0} = 100\right)$

NLT_{33}. Again, we suspect this to be essentially a consequence of invoking turbulence isotropy to develop several closures within the model. An overprediction is observed for C_{11}, next to the wall, at $DR = 18$ %, which decreases when DR increases to $DR = 37$ %. For the C_{12} component there are also large discrepancies, with an overprediction next to the wall and a underprediction away from wall, which becomes stronger at large DR. The predictions of C_{22} are fair due to the correct prediction of NLT_{22}, but deficiencies observed with NLT_{22} are carried over to C_{22}, for example the underprediction of the maximum value of NLT_{22} is also detected in C_{22}. The behavior in terms of the trace C_{kk} can be assessed indirectly through function $f(C_{kk})$ plotted in Fig. 3; there is an overprediction of the maximum value of $f(C_{kk})$ at both $DR = 18$ % and 37 %.

The transverse distributions of the three shear stresses for $DR = 18$ % and 37 % are compared in Fig. 13 with the corresponding DNS data. The solvent stress is always well predicted and this is a consequence of the correct prediction of the velocity profile. The reduction of the Reynolds stress with DR and the simultaneous presence of a polymer stress is clear, but close to the wall there is an under-prediction of $-\rho\overline{uv}$ and an over-prediction of τ_{xy}^{p}, whereas away from the wall the opposite occurs. The polymer shear stress is calculated from the shear component of the conformation tensor and these differences are due to the corresponding predictions of C_{xy}. Since the total shear stress must follow the straight line imposed by the pressure gradient for fully-developed channel flow, the discrepancies in the prediction of the Reynolds shear stress must compensate the deficiencies in polymer shear stress.

Ultimately, the evolution of the conformation and polymer stress tensors are based on the model used for NLT_{ij}. Since the closure used for this tensor in this k-ω model is the same as in the k-ε model of Resende et al. [21], it is no surprise that the stress distributions are essentially identical.

4 Conclusions

A k-ω turbulence model was developed for viscoelastic fluids described by the FENE-P rheological constitutive equation. It is based on the low-Reynolds number k-ω model of Bredberg et al. [30] for Newtonian fluids, which was extended as follows: the eddy viscosity and NLT_{ij} closures are mathematically transformed from the corresponding closures developed in the context of the k-ε model of Resende et al. [21]; the closures for the cross-diffusion term, the destruction of ω^N and the viscoelastic turbulent diffusion contain specific developments, even though they get inspiration from those of Resende et al. [21].

The performance of the model was assessed first through comparisons with DNS data for $Re_{\tau 0} = 395$, $L^2 = 900$ and $\beta = 0.9$ at $We_{\tau 0} = 25$ ($DR = 18$ %) and $We_{\tau 0} = 100$ ($DR = 37$ %) and also with the predictions of the k-ε model of Resende et al. [21] for the same flow conditions and with the expression of Li et al. [9] for the variation of DR with Weissenberg number obtained from a large set of DNS data.

The k-ω model predictions of the mean velocity were nearly identical to those of the k-ε model of Resende et al. [21] but as we increase flow elasticity to the intermediate DR regime the k-ω model behaves better, especially when increasing the maximum molecular extensibility. For the other quantities (k, ε^V,NLT_{ij}) generally

speaking there was an improvement relative to those of Resende et al. [21] especially for the intermediate DR region, and most notoriously for the prediction of k, which was closer to the DNS data, but still not enough to eliminate the under-prediction of k. The under-prediction of k limits the application of this turbulence model to drag reductions below about 47 %, a value at which the deviation in relation to the correlation of Li et al. [9] reaches 10 %, as is also the case with the $k-\varepsilon$ model of Resende et al. [21]. We believe this is a limitation of two-equation turbulence models associated with the assumption of turbulence isotropy, because there is an incompatibility between the variations of eddy viscosity and k with drag reduction: k increases and the eddy viscosity decreases at low DR, whereas this type of closure implies $\nu_T \propto k$. The solution of this deficiency requires closures that do not directly couple the eddy viscosity with the turbulent kinetic energy. This can be achieved in a number of ways: through adopting a Reynolds stress model where the direct link between the Reynolds stress and k is not imposed (using a Reynolds stress model developed from a simple toy rheological constitutive equation Resende et al. [39] were able to achieve the high drag reduction regime) or also as in k-ε-v^2-f models where the eddy viscosity depends on two different turbulent velocity scales. Future work involves the extension of the turbulence model to all regimes of turbulent drag reduction and the substitution of the friction velocity by a local velocity scale in the closures to allow the extension of the model to other scenarios, such as free stream flows.

Appendix: Equations of the k-ω turbulence model of Bredberg et al. [30] for Newtonian fluids

The eddyviscosity required to calculate the Reynolds stress in Eq. 8 is given by Eq. 33

$$\nu_T = C_\mu \times f_\mu \times \frac{k}{\omega} \tag{33}$$

where k and ω are to be computed by the transport Eqs. 34 and 35, respectively using the damping function of Eq. 36.

$$\frac{Dk}{Dt} = P_k - C_k \omega k + \frac{\partial}{\partial x_i}\left[\left(\nu + \frac{\nu_T}{\sigma_k}\right)\frac{\partial k}{\partial x_i}\right] \tag{34}$$

$$\frac{D\omega}{Dt} = \frac{\partial}{\partial x_i}\left[\left(\nu + \frac{\nu_T}{\sigma_\omega}\right)\frac{\partial \omega}{\partial x_i}\right] + C_{\omega_1}\frac{\omega}{k}P_k - C_{\omega_2}\omega^2 + \frac{C_\omega}{k}(\nu + \nu_T)\frac{\partial k}{\partial x_i}\frac{\partial \omega}{\partial x_i} \tag{35}$$

$$f_\mu = 0.09 + \left(0.91 + \frac{1}{R_t^3}\right)\left[1 - \exp\left\{-\left(\frac{R_t}{28}\right)^{2.75}\right\}\right] \text{ with } R_t = \frac{k}{\omega \cdot \nu} \tag{36}$$

Acknowledgements The authors gratefully acknowledge funding from FEDER and FCT through Projects POCI/56342/EQU/2004, PTDC/EME-MFE/113589/2009 and SFRH/BD/18475/2004. K.K. would like to acknowledge the support from KISTI Supercomputing Center (No. KSC-2009-S02-0013). RS is grateful to NSF for grant CBET 1055219.

References

1. Sureshkumar, R., Beris, A.N., Handler, R.A.: Direct numerical simulation of the turbulent channel flow of a polymer solution. Phys. Fluids **9**(3), 743–755 (1997)
2. Angelis, E.D., Casciola, C.M., Piva, R.: DNS of wall turbulence: dilute polymers and self-sustaining mechanisms. Comput. Fluids **31**, 495–507 (1999)
3. Li, C.F., Sureshkmar, R., Khomami, B.: Influence of rheological parameters on polymer induced turbulent drag reduction. J. Non-Newton. Fluid Mech. **140**, 23–40 (2006)
4. Housiadas, K.D., Beris, A.N.: An efficient fully implicit spectral scheme for DNS of turbulent viscoelastic channel flow. J. Non-Newton. Fluid Mech. **122**, 243–262 (2004)
5. Dimitropoulos, C.D., Sureshkumar, R., Beris, A.N.: Direct numeric simulation of viscoelastic turbulent channel flow exhibiting drag reduction: effect of variation of rheological parameters. J. Non-Newton. Fluid Mech. **79**, 433–468 (1998)
6. Yu, B., Kawaguchi, Y.: Effect of Weissenberg number on the flow structure: DNS study of drag reducing flow with surfactant additives. Int. J. Heat Fluid Flow **24**, 491–499 (2003)
7. Yu, B., Kawaguchi, Y.: Parametric study of surfactant-induced drag-reduction by DNS. Int. J. Heat Fluid Flow **27**, 887–894 (2006)
8. Dimitropoulos, C.D., Sureshkumar, R., Beris, A.N., Handler, R.A.: Budgets of Reynolds stress, kinetic energy and streamwise entrophy in viscoelastic turbulent channel flow. Phys. Fluids **13**(4), 1016–1027 (2001)
9. Li, C.F., Gupta, V.K., Sureshkmar, R., Khomami, B.: Turbulent channel flow of dilute polymeric solutions: drag reduction scaling and an eddy viscosity model. J. Non-Newton. Fluid Mech. **139**, 177–189 (2006)
10. Housiadas, K.D., Beris, A.N., Handler, R.A.: Viscoelastic effects on higher order statistics and coherent structures in turbulent channel flow. Phys. Fluids **17**(35106) (2005)
11. Kim, K., Li, C.F., Sureshkumar, R., Balachandar, S., Adrian, R.: Effects of polymer stresses on eddy structures in drag-reduced turbulent channel flow. J. Fluid Mech. **584**, 281–299 (2007)
12. Pinho, F.T., Li, C.F., Younis, B.A., Sureshkumar, R.: A low Reynolds number k-ε turbulence model for FENE-P viscoelastic fluids. J. Non-Newton. Fluid Mech. **154**, 89–108 (2008)
13. Malin, M.R.: Turbulent pipe flow of power-law fluids. Int. Commun. Heat Mass Transfer **24**(7), 977–988 (1997)
14. Pinho, F.T.: A GNF framework for turbulent flow models of drag reducing fluids and proposal for a k-ε type closure. J. Non-Newton. Fluid Mech. **114**, 149–184 (2003)
15. Cruz, D.O.A., Pinho, F.T.: Turbulent pipe flow predictions with a low Reynolds number k-ε model for drag reducing fluids. J. Non-Newton. Fluid Mech. **114**, 109–148 (2003)
16. Cruz, D.O.A., Pinho, F.T., Resende, P.R.: Modeling the new stress for improved drag reduction predictions of viscoelastic pipe flow. J. Non-Newton. Fluid Mech. **121**, 127–141 (2004)
17. Resende, P.R., Escudier, M.P., Presti, F., Pinho, F.T., Cruz, D.O.A.: Numerical predictions and measurements of Reynolds normal stresses in turbulent pipe flow of polymers. Int. J. Heat Fluid Flow **27**, 204–219 (2006)
18. Ptasinski, P.K., Boersma, B.J., Nieuwstadt, F.T.M., Hulsen, M.A., Brule, B.H.A.A.V.D., Hunt, J.C.R.: Turbulent channel flow near maximum drag reduction: simulation, experiments and mechanisms. J. Fluid Mech. **490**, 251–291 (2003)
19. Nagano, Y., Hishida, M.: Improved form of the k-ε model for wall turbulent shear flows. J. Fluids Eng. **109**, 156–160 (1987)
20. Nagano, Y., Shimada, M.: Modeling the dissipation-rate equation for two-equation turbulence model. In: Ninth symposium on "Turbulent shear flows", Kyoto, Japan, 16–18 August (1993)
21. Resende, P.R., Kim, K., Younis, B.A., Sureshkumar, R., Pinho, F.T.: A k-ε turbulence model for FENE-P fluid flows at low and intermediate regimes of polymer-induced drag reduction. J. Non-Newton. Fluid Mech. **166**, 639–660 (2011)
22. Iaccarino, G., Shaqfeh, E.S.G., Dubief, Y.: Reynolds-averaged modeling of polymer drag reduction in turbulent flows. J. Non-Newton. Fluid Mech. **165**, 376–384 (2010)
23. Durbin, P.A.: Separated flow computations with the k-ε-v2 model. AIAA J. **33**, 659–664 (1995)
24. Wilcox, D.C.: Turbulence modeling for CFD, 1st edn. DCW Industries Inc., La Cañada, California (1993)
25. Wilcox, D.: Reassessment of the scale-determining equation for advanced turbulence models. AIAA J. **26**, 1299–1310 (1988)
26. Menter, F.R.: Influence of freestream values on k-ε turbulence model predictions. AIAA J. **30**(6), 1657–1659 (1991)

27. Speziale, C.G., Abid, R., Anderson, E.C.: Critical evaluation of two-Equation models for near-Wall turbulence. AIAA J. **30**(2), 324–331 (1992)
28. Menter, F.R.: Two-equation eddy-viscosity turbulence models for engineering applications. AIAA J. **32**(8), 1598–1604 (1994)
29. Peng, S.-H., Davidson, L., Holmberg, S.: A modified low-Reynolds-number k-ω model for recirculating flows. J. Fluids Eng. **119**, 867–875 (1997)
30. Bredberg, J., Peng, S.H., Davidson, L.: An improved k-ω turbulence model applied to recirculating flows. Int. J. Heat Fluid Flow **23**, 731–743 (2002)
31. Abe, K., Kondoh, T., Nagano, Y.: A new turbulence model for predicting fluid flow and heat transfer in separating and reattaching flows—I. Flow field calculations. Int. J. Heat Mass Transfer **37**, 139–151 (1994)
32. Wilcox, D.: Comparison of two-equation turbulence models for boundary ayers with pressure gradient. AIAA J. **31**, 1414–1421 (1993)
33. Lien, F., Kalitzin, G.: Computations of transonic flow with the v2-f turbulence model. Int. J. Heat Fluid Flow **22**, 53–61 (2001)
34. Bird, R.B., Armstrong, R.C., Hassager, O.: Dynamics of Polymeric Liquids, vol. 1: Fluids Mechanics, 2nd edn. Wiley, New York (1987)
35. Bird, R.B., Armstrong, R.C., Hassager, O.: Dynamics of Polymeric Liquids, vol. 2: Kinetic Theory, 2nd edn. Wiley, New York (1987)
36. Resende, P.R.: Turbulence models for viscoelastic fluids. PhD thesis, University of Porto (2010)
37. Housiadas, K.D., Beris, A.N.: Polymer-induced drag reduction: Effects of the variations in elasticity and inertia in turbulent viscoelastic channel flow. Phys. Fluids **15**(8), 2369–2384 (2003)
38. Younis, B.A.: EXPRESS: A Computer Programme for Two-Dimensional Turbulent Boundary Layer Flow. Departament of Civil Engineering, City University, London, UK (1987)
39. Resende, P.R., Pinho, F.T., Cruz, D.O.A.: A Reynolds stress model for turbulent pipe flow of viscoelastic fluids. Paper presented at the Proceedings of the First National Conference on Numerical Methods for Fluid Mechanics and Thermodynamics, Costa da Caparica, Lisboa, Portugal, 8–9 June 2006